

# Doppler Estimation for High-Velocity Targets Using Subpulse Processing and the Classic Chinese Remainder Theorem

Fernando Darío Almeida García, André Saito Guerreiro, Gustavo Rodrigues de Lima Tejerina, José Cândido S. Santos Filho, Gustavo Fraidenaich, and Michel Daoud Yacoub, *Member, IEEE*

**Abstract**—In pulsed Doppler radars, the classic Chinese remainder theorem (CCRT) is a common method to resolve Doppler ambiguities caused by fast-moving targets. Another issue concerning high-velocity targets is related to the loss in the signal-to-noise ratio (SNR) after performing *range compression*. In particular, this loss can be partially mitigated by the use of subpulse processing (SP). Modern radars combine these techniques in order to reliably unfold the target velocity. However, the presence of background noise may compromise the Doppler estimates. Hence, a rigorous statistical analysis is imperative. In this work, we provide a comprehensive analysis on Doppler estimation. In particular, we derive novel closed-form expressions for the probability of detection (PD) and probability of false alarm (PFA). To this end, we consider the newly introduced SP along with the CCRT. A comparison analysis between SP and the classic pulse processing (PP) technique is also carried out. Numerical results and Monte-Carlo simulations corroborate the validity of our expressions and show that the SP-plus-CCRT technique helps to greatly reduce the PFA compared to previous studies, thereby improving radar detection.

**Index Terms**—Classic Chinese remainder theorem, robust Chinese remainder theorem, Doppler frequency estimation, subpulse processing, probability of detection.

## I. INTRODUCTION

One important concern in modern pulsed radars is related to the Doppler frequency estimation of fast-velocity targets. Due to the high target's radial velocity, ambiguous estimates are more likely to occur. More specifically, ambiguous estimates appear whenever the target's Doppler shift is greater than the pulse repetition frequency (PRF) [1]. It seems obvious to think that increasing the PRF will overcome this problem. However, if we are interested in detecting targets located at long distances, then the PRF will be restricted to a maximum value. Therefore, the choice of PRF is a trade-off between range and Doppler requirements [2]. Fortunately, there are some techniques that can resolve ambiguities, although at the cost of extra measurement time and processing load. These techniques make use of multiples PRFs [3]–[7]. The most known and used technique is the classic Chinese remainder theorem (CCRT). The CCRT is a fast and accurate method to resolve the unambiguous Doppler frequency. This is accomplished by solving a

set of congruences, formed by the estimated measurements of each PRF [7]–[9]. Nevertheless, in this method, the number of PRFs will not be sufficient to resolve a certain quantity of targets. In general,  $L$  PRFs are required to successfully disambiguate  $L - 1$  targets. If the number of targets exceeds  $L - 1$ , then *ghosts* can appear.<sup>1</sup> Unless additional data (e.g., tracking information) is available, the radar has no way of recognizing possible false detections [4]. Care must be taken in the analysis and design since the number of PRFs and the number of targets to be detected have a direct relationship.

Another issue concerning high-velocity targets is related to the signal-to-noise ratio (SNR) loss. This occurs because the Doppler shift of fast-moving targets will provoke a mismatch between the received signal and its replica [2]. Consequently, the SNR after *range compression* may be drastically reduced.<sup>2</sup> Some radar systems estimate and remove the Doppler shift prior to applying *range compression*. Nonetheless, some residual or uncompensated Doppler typically remains. This concern was partially alleviated in [11], [12]. Specifically, in [11], the authors proposed a subpulse processing (SP), which proved to have a higher Doppler tolerance,<sup>3</sup> increasing the ability to detect fast-moving targets. The shortcomings of SP are computation time (critical for most radars), processing load, and poor velocity resolution.

As stated before, the CCRT and SP have hardware and physical limitations when it comes to estimating high target velocities. In practice, modern pulsed radars take advantage of these two techniques so as to improve the system's capability to accurately detect the target's true Doppler frequency. Since SP the CCRT are affected by the presence of background noise, then a thorough statistical analysis involving these two estimation techniques must be carried out. Recently in [14], the authors proposed a novel expression for the probability to correctly estimate the unambiguous Doppler frequency considering the CCRT and the common pulse processing (PP) technique [2]. However, to the best of our knowledge, there is no performance analysis considering the SP-plus-CCRT technique.

The main objective of this research is to combine the statisti-

F. D. A. García, A. S. Guerreiro, G. R. de Lima Tejerina, J. C. S. Santos Filho, G. Fraidenaich, and M. D. Yacoub are with the Wireless Technology Laboratory, Department of Communications, School of Electrical and Computer Engineering, University of Campinas, 13083-852 Campinas, SP, Brazil, Tel: +55(19)3788-5106, e-mail: {ferdardal, andsaito, tejerina, candido, gf, michel}@decom.fee.unicamp.br.

<sup>1</sup>*Ghosts* are false targets resulting from false coincidences of Doppler-ambiguous or range-ambiguous data [4].

<sup>2</sup>*Range compression* refers to the convolution operation between the received signal and the replica of the transmitted signal [10].

<sup>3</sup>Doppler tolerance refers to the degree of degradation in the compressed response due to uncompensated Doppler [13].

cal analysis conducted in [14] along with the newly introduced SP and the CCRT. To do so, we adopt a stochastic model that suits our Doppler estimation techniques. Then, we derive novel and closed-form expressions for: **i)** the probability to correctly estimate the Doppler frequency, also called probability of detection (PD); and **ii)** the probability to erroneously estimate the Doppler frequency, also called probability of false alarm (PFA).

The remainder of this paper is organized as follows. Section II introduces some key concepts to understand how the velocity estimation is performed. Section III describes the system model. Section IV analyzes the Doppler estimation using multiple PRFs; Section V discusses the representative numerical results. Finally, Section VI concludes this paper.

In what follows,  $(a) \bmod(b)$  denotes the remainder of the euclidean division of  $a$  by  $b$ ;  $|\cdot|$ , absolute value;  $\lfloor \cdot \rfloor$ , floor operation;  $\text{round}(\cdot)$ , rounding operation;  $\text{Pr}[\cdot]$ , probability;  $\mathbb{E}(\cdot)$ , expectation;  $\text{Var}(\cdot)$ , variance;  $(\cdot)^*$ , complex conjugate;  $\cap$ , intersection of events;  $\cup$ , union of events;  $\mathcal{N}(\mu, \sigma^2)$  denotes a Gaussian distribution with mean  $\mu$  and variance  $\sigma^2$ ;  $\mathcal{N}_c(\mu, \sigma^2)$  denotes a complex Gaussian distribution with mean  $\mu$  and variance  $\sigma^2$ , and  $j = \sqrt{-1}$  is the imaginary unit.

## II. PRELIMINARIES

In this section, we present a brief introduction about the PP and SP techniques. Latter, we describe the basis to understand the CCRT algorithm. Finally, we show how the combined technique SP-plus-CCRT works in order to improve Doppler estimation.

### A. Pulse Processing

PP is the common technique employed by the radar to estimate the target velocity and improve the SNR. In this processing technique, the radar transmits a sequence of  $M$  pulses during a coherent processing interval (CPI) [15]. Then, *range compression* is performed on each pulse to improve the radar's range resolution. Finally, the discrete Fourier transform (DFT) is applied along the slow-time samples to increase the SNR and to estimate the target Doppler frequency [2]. These samples are collected at a rate equal to the PRF. The maximum Doppler frequency shift that the radar manages to detect using PP is  $\Psi_{max} = \pm \text{PRF}/2$ . If the target Doppler frequency,  $f_d$ , exceeds this value, then the radar will deliver ambiguous Doppler measurements. The Doppler frequency shift will be positive for closing targets and negative for receding targets. The target velocity,  $v_t$ , and its corresponding Doppler shift are related by the following equation [16]:

$$f_d = \frac{2v_t f_R}{c} = \frac{2v_t}{\lambda}, \quad (1)$$

where  $f_R$  is the radar's operation frequency,  $c$  is the speed of light, and  $\lambda$  is the radar frequency.

### B. Subpulse Processing

SP improves Doppler tolerance by mitigating the loss in SNR caused by the uncompensated Doppler shift of fast-moving targets [2], [11]. Moreover, SP is used to overcome

the problem of ambiguous Doppler measurements. The SP algorithm runs as follows:

- 1) First, the replica of the transmitted signal is divided into  $N$  subpulses – unlike PP that used the entire replica.
- 2) Latter, *range compression* is carried out between each subpulse and the received signal (cf. [11], [12] for a detailed discussion on this). The use of shorter replicas will enhance the system's Doppler tolerance [10], increasing the detection capability of fast-moving targets. Of course, this process leads to a reduction in the peak amplitude of the sub-compression response (by a factor of  $1/N$ ). Here, the slow-time samples are collected at a rate of  $\Phi = N/\tau$ , where  $\tau$  is the pulse width. It is important to emphasize that PP and SP are performed simultaneously, that is, for each of the  $M$  compressions, the radar carried out  $N$  sub-compressions [12].
- 3) Finally, the slow-time samples are coherently integrated to estimate the target Doppler frequency and to “restore” the peak amplitude of the sub-compression response.

The number of subpulses can be chosen as high as needed, as long as it is taken into consideration that each additional subpulse requires an extra *range compression* operation, increasing the computational load and computation time. The maximum Doppler frequency shift that the radar can now manage to detect is  $\Phi_{max} = \pm N/2\tau$  [11]. Since  $\Phi_{max} > \Psi_{max}$ , SP provides a higher frequency range of detection for fast-moving targets.

Computation time is critical for most radars and depends strongly on the radar's operation mode (e.g. tracking, searching or imaging), thereby limiting the number of subpulses. Commonly, the number of subpulses is set between 5 and 10. However, this small number yields to a poor discretization in the frequency domain and, consequently, producing inaccurate estimates.

### C. Classic Chinese Remainder Theorem

The use of multiples PRFs is a common approach to resolve range and Doppler ambiguities [3], [4], [8], [17]. In this work, we only focus on solving Doppler ambiguities. Consider for the moment a target with Doppler shift  $f_d > \Psi_{max}$ . In this scenario, the radar will detect the target with an apparent Doppler shift,  $f_{d_{ap}}$ , that satisfies

$$f_d = f_{d_{ap}} + n\text{PRF}, \quad (2)$$

where  $n$  is some integer. It is convenience to express the target's Doppler shift  $f_d$  in terms of its corresponding Doppler bin,  $b_d$ . Thus, (2) becomes

$$b_d = b_{ap} + nM, \quad (3)$$

in which  $b_{ap} \in \{0, 1, 2, \dots, M-1\}$  is the apparent Doppler bin, defined as

$$b_{ap} = \left\lfloor \left\lfloor \frac{f_{d_{ap}}}{\Delta D} \right\rfloor \right\rfloor, \quad f_{d_{ap}} \geq 0 \quad (4)$$

$$b_{ap} = M - \left\lfloor \left\lfloor \frac{f_{d_{ap}}}{\Delta D} \right\rfloor \right\rfloor, \quad f_{d_{ap}} < 0 \quad (5)$$

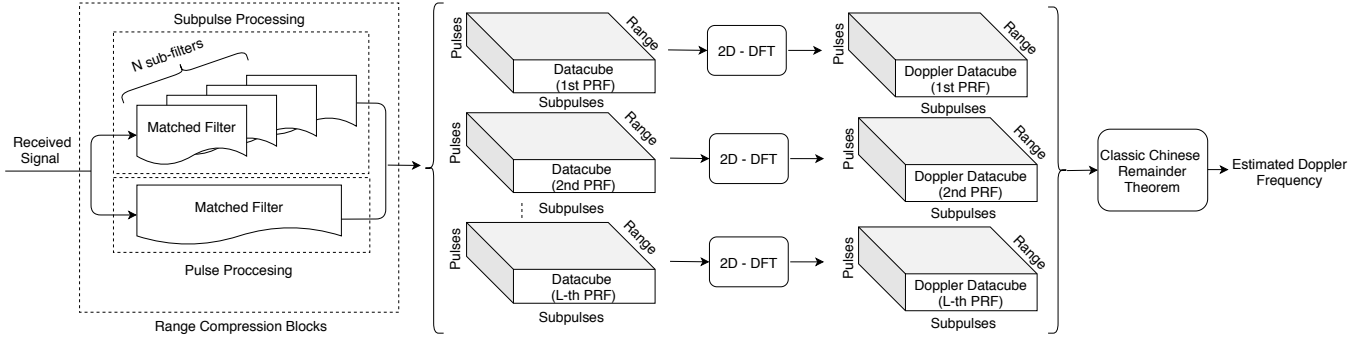


Fig. 1: Block diagram for Doppler estimation.

with  $\Delta D = \text{PRF}/M$  being the Doppler bin spacing. Under this scenario, the radar is incapable to detect the target's true Doppler frequency.

Now, suppose that we have  $L$  PRFs. Then, the unambiguous target's Doppler bin must satisfies the following congruences:

$$b_d \equiv b_{ap_i} + n_i M_i, \quad 1 \leq i \leq L \quad (6)$$

The CCRT states that if all PRFs are pairwise coprimes, then the set of congruences in (6) will have a unique solution given by [4], [17], [18]

$$b_d = \left( \sum_{i=1}^L b_{ap_i} \beta_i \right) \text{mod}(\Theta), \quad (7)$$

where  $\Theta = \prod_{i=1}^L M_i$ ,  $\beta_i = b_i \Theta / \text{PRF}_i$ , and  $b_i$  is the smaller integer which can be computed by solving the following expression:

$$\left( \frac{b_i \Theta}{M_i} \right) \text{mod}(M_i) = 1. \quad (8)$$

#### D. Doppler Estimation

Fig. 1 depicts the entire block diagram for Doppler estimation. First, the received signal passes through two types of independent *range compression* blocks, one for PP and one for SP. This process is performed in sequence for each pulse repetition interval (PRI). The outputs of both blocks are combined and stored in memory to form a datacube [2]. (The datacube's data is organized by range, number of pulses, and number of subpulses.) More datacubes are needed when using more than one PRF, as shown in Fig. 1. Next, a 2D-DFT block is applied to each datacube to perform coherent integration. (The 2D-DFT block is referred to as a two-dimensional DFT applied along with pulses and subpulses.) Latter, the output of the 2D-DFT block is a matrix with the same size containing the estimated Doppler shifts. This new matrix is referred to as Doppler datacube. Finally, the CCRT is applied over the Doppler datacubes. This process will be clarified in Section V by means of simulation.

Noise, jammer, and clutter are major concerns in all radar systems. In this work, we consider the presence complex white Gaussian noise (CWGN). Thus, the Doppler spectrum of fast moving targets will be compromised due to the intrinsic characteristics of noise. For example, a high noise power could

mask small target returns, degrading radar performance. Even if the target return is entirely deterministic, the combined signal (target-plus-noise) is a random process and must be treated as such. Therefore, we need to assess the statistics underlying Doppler analysis, but first, we need to come up with a specific stochastic model that suits the requirements and design of our radar's estimation scheme. This is discussed in the next section.

### III. SYSTEM MODEL

In this section, we propose a stochastic model that fits our signal processing schemes. In addition, we describe the premises (hypotheses) used for Doppler estimation.

According to Sections II-A and II-B, the collected signals in the slow-time domain corresponding to PP and SP can be expressed, respectively, as

$$\begin{aligned} g_1[m] &= s_1[m] + w_1[m] \\ &= a_1 \exp(j2\pi f_d m / \text{PRF}) + w_1[m], \quad 0 \leq m \leq M-1 \\ g_2[n] &= s_2[n] + w_2[n] \\ &= a_2 \exp(j2\pi f_d n / \Phi) + w_2[n], \quad 0 \leq n \leq N-1 \end{aligned} \quad (9)$$

where  $s_1[m]$  and  $s_2[n]$  are discrete complex sine signals<sup>4</sup> originated by changes in the target position;  $w_1[m]$  and  $w_2[n]$  are discrete additive complex Gaussian noises; and finally,  $a_1$  and  $a_2$  are the amplitudes at the output of the matched filters. Depending on the target velocity, the output amplitudes  $a_1$  and  $a_2$  maybe be greatly attenuated. However, the attenuation in  $a_2$  is partially mitigated by the use of SP. In particular, it follows that  $a_2 > a_1$  for high-velocity targets [11]. Additionally, we define  $2\sigma_{t_1}^2$  and  $2\sigma_{t_2}^2$  as the total mean powers – in the time domain – for  $w_1[m]$  and  $w_2[n]$ , respectively. As seen in practice, and due to the stationary characteristic of noise, we have that  $\sigma_{t_1}^2 = \sigma_{t_2}^2$  [19]. However, we will remain using separate notations for  $\sigma_{t_1}^2$  and  $\sigma_{t_2}^2$  so as to distinguish the noise power from PP and SP. Of course, these separate notations will not alter, in any form, our performance analysis.

<sup>4</sup>In most systems, the radio frequency (RF) signal is mixed to baseband prior to compression, and a coherent detector is used in the downconversion process to form in-phase (I) and quadrature (Q) receive channels, thereby creating a complex baseband signal.

The SNR measured in the time domain considering PP and SP, can be expressed, respectively, as

$$\text{SNR}_{t_1} = \frac{|a_1|^2}{2\sigma_{t_1}^2} \quad (11)$$

$$\text{SNR}_{t_2} = \frac{|a_2/N|^2}{2\sigma_{t_2}^2}. \quad (12)$$

Observe in (12) that the fact of dividing the replica into  $N$  subpulses causes a reduction in the SNR by a factor of  $1/N^2$ , as mentioned in Section II-B.

The DFT is the primary operation to implement coherent integration. More precisely, the DFT provides a mechanism to test multiple candidate frequencies to maximize the *integration gain* [2]. The corresponding DFTs for (9) and (10) are given, respectively, by

$$\begin{aligned} G_1[k'] &\triangleq \mathcal{F}\{g_1[m]\} \\ &= \sum_{m=0}^{M-1} g_1[m] \exp(-j2\pi k'm/M) \\ &= S_1[k'] + W_1[k'], \quad 0 \leq k' \leq M-1 \end{aligned} \quad (13)$$

$$\begin{aligned} G_2[l'] &\triangleq \mathcal{F}\{g_2[n]\} \\ &= \sum_{n=0}^{N-1} g_2[n] \exp(-j2\pi l'n/N) \\ &= S_2[l'] + W_2[l'], \quad 0 \leq l' \leq N-1 \end{aligned} \quad (14)$$

The SNR measured in the frequency domain considering PP and SP, are given, respectively, by [2, Eq. (17.37)]

$$\text{SNR}_1 = \frac{|Ma_1|^2}{2\sigma_1^2} \quad (15)$$

$$\text{SNR}_2 = \frac{|a_2|^2}{2\sigma_2^2}, \quad (16)$$

in which  $\sigma_1^2 = M\sigma_{t_1}^2$  and  $\sigma_2^2 = N\sigma_{t_2}^2$  are half of the noise powers – in the frequency domain – for  $W_1[k']$  and  $W_2[l']$ , respectively.

The Doppler estimates are based on the absolute values of  $G_1[k']$  and  $G_2[l']$ . That is, (13) and (14) will provide estimates for  $f_d$ , say  $\hat{f}_1$  and  $\hat{f}_2$ , by searching  $k'$  and  $l'$ , in which the absolute values of  $G_1[k']$  and  $G_2[l']$  are maximum. It is worth mentioning that if  $\Psi_{max} < f_d$  and  $\Phi_{max} < f_d$ , then  $\hat{f}_1$  and  $\hat{f}_2$  will display ambiguous Doppler estimates.

Now, considering  $L$  PRFs (say,  $\text{PRF}_1, \dots, \text{PRF}_L$ ), we can define the absolute values for  $G_1[k']$  and  $G_2[l']$  at the  $i$ -th PRF, respectively, as

$$H_{1,i}[k'] \triangleq |G_{1,i}[k']| \quad 0 \leq k' \leq M_i - 1 \quad (17)$$

$$H_{2,i}[l'] \triangleq |G_{2,i}[l']| \quad 0 \leq l' \leq N_i - 1 \quad (18)$$

where the subscript  $i \in \{1, \dots, L\}$  denotes the association to the  $i$ -th PRF.

Herein, we assume that  $G_{1,i}[k']$  is composed of  $M_i - 1$  independent and identically distributed noise samples and one target-plus-noise sample, denoted as  $\mathcal{G}_{1,i}$ . On the other hand,  $G_{2,i}[l']$  is composed of  $N_i - 1$  independent and identically distributed noise samples and one combined sample, denoted

as  $\mathcal{G}_{2,i}$ . The target-plus-noise samples  $\mathcal{G}_{1,i}$  and  $\mathcal{G}_{2,i}$  can be modeled, respectively, by [20, Eq. (1)]

$$\begin{aligned} \mathcal{G}_{1,i} &= \sigma_{1,i} \left( \sqrt{1 - \lambda_{1,i}^2} A_{1,i} + \lambda_{1,i} A_{0,i} \right) \\ &\quad + j\sigma_{1,i} \left( \sqrt{1 - \lambda_{1,i}^2} B_{1,i} + \lambda_{1,i} B_{0,i} \right) \end{aligned} \quad (19)$$

$$\begin{aligned} \mathcal{G}_{2,i} &= \sigma_{2,i} \left( \sqrt{1 - \lambda_{2,i}^2} A_{2,i} + \lambda_{2,i} A_{0,i} \right) \\ &\quad + j\sigma_{2,i} \left( \sqrt{1 - \lambda_{2,i}^2} B_{2,i} + \lambda_{2,i} B_{0,i} \right), \end{aligned} \quad (20)$$

where  $A_{p,i}$  and  $B_{p,i}$  ( $p = 1, 2$ ) are mutually independent random variables (RVs) distributed as  $\mathcal{N}(0, \frac{1}{2})$ , and  $\lambda_{p,i} \in (0, 1]$ . Then, for any  $p$  and  $q$  ( $q = 1, 2$ ), it follows that  $\mathbb{E}(A_{p,i}B_{q,i}) = 0$  and  $\mathbb{E}(A_{p,i}A_{q,i}) = \mathbb{E}(B_{p,i}B_{q,i}) = \frac{1}{2}\delta_{pq}$ . ( $\delta_{pq} = 1$  if  $p = q$ , and  $\delta_{pq} = 0$  otherwise.) In addition,  $A_{0,i}$  and  $B_{0,i}$  are mutually independent RVs distributed as  $\mathcal{N}(m_{\text{Re},i}, \frac{1}{2})$  and  $\mathcal{N}(m_{\text{Im},i}, \frac{1}{2})$ , respectively. Thus,  $\mathcal{G}_{1,i}$  and  $\mathcal{G}_{2,i}$  are non-zero mean complex Gaussian RVs with probability density functions (PDFs) given, respectively, by  $\mathcal{N}_c(\lambda_{1,i}(m_{\text{Re},i} + jm_{\text{Im},i}), \sigma_{1,i}^2)$  and  $\mathcal{N}_c(\lambda_{2,i}(m_{\text{Re},i} + jm_{\text{Im},i}), \sigma_{2,i}^2)$ . The correlation coefficient between any pair of  $(\mathcal{G}_{1,i}, \mathcal{G}_{2,i})$ , can be calculated as [20, Eq. (2)]

$$\begin{aligned} \rho_{kl,i} &\triangleq \frac{\mathbb{E}(\mathcal{G}_{1,i}\mathcal{G}_{2,i}^*) - \mathbb{E}(\mathcal{G}_{1,i})\mathbb{E}(\mathcal{G}_{2,i}^*)}{\sqrt{\text{Var}(\mathcal{G}_{1,i})\text{Var}(\mathcal{G}_{2,i}^*)}} \\ &= \lambda_{1,i}\lambda_{2,i}. \end{aligned} \quad (21)$$

This correlation exists because both PP and SP use the same received signal when performing *range compression* [2]. Observe that the parameters  $\lambda_{1,i}^2$ ,  $\lambda_{2,i}^2$ ,  $m_{\text{Re},i}$  and  $m_{\text{Im},i}$  can be used to model the compressed responses  $|M_i a_{1,i}|^2$  and  $|a_{2,i}|^2$ . This can be done by making the following substitutions:  $|M_i a_{1,i}|^2 = \lambda_{1,i}^2(m_{\text{Re},i}^2 + m_{\text{Im},i}^2)$  and  $|a_{2,i}|^2 = \lambda_{2,i}^2(m_{\text{Re},i}^2 + m_{\text{Im},i}^2)$ . On the other hand,  $\lambda_{1,i}$  and  $\lambda_{2,i}$  can be chosen to meet a desired correlation coefficient.

By the above, it follows that  $H_{1,i}[k']$  is composed of  $M_i - 1$  Rayleigh distributed samples, denoted as  $X_{k,i}$  ( $k \in \{1, 2, \dots, M_i - 1\}$ ), and one Rice distributed sample, denoted as  $R_{1,i}$ . Similarly,  $H_{2,i}[l']$  is composed of  $N_i - 1$  Rayleigh distributed samples, denoted as  $Y_{l,i}$  ( $l \in \{1, 2, \dots, N_i - 1\}$ ), and one Rice distributed sample, denoted as  $R_{2,i}$ . The PDFs of  $X_{k,i}$  and  $Y_{l,i}$  are given, respectively, by

$$f_{X_{k,i}}(x_{k,i}) = \frac{x_{k,i} \exp\left(-\frac{x_{k,i}^2}{2\sigma_{k,i}^2}\right)}{\sigma_{k,i}} \quad (22)$$

$$f_{Y_{l,i}}(y_{l,i}) = \frac{y_{l,i} \exp\left(-\frac{y_{l,i}^2}{2\sigma_{l,i}^2}\right)}{\sigma_{l,i}}. \quad (23)$$

Moreover, since  $R_{2,i}$  and  $R_{2,i}$  bear a certain degree of correlation, they are governed by a bivariate Rician distribution,

given by [20], [21]

$$f_{R_{1,i}, R_{2,i}}(r_{1,i}, r_{2,i} | \mathcal{H}_1) = \int_0^\infty \exp(-t\xi_i) \times \exp(-\mathbf{m}_i) I_0(2\sqrt{\mathbf{m}_i}t) \prod_{p=1}^2 \frac{r_{p,i}}{\Omega_{p,i}^2} \times \exp\left(-\frac{r_{p,i}^2}{2\Omega_{p,i}^2}\right) I_0\left(\frac{r_{p,i}\sqrt{t\sigma_{p,i}^2\lambda_{p,i}^2}}{\Omega_{p,i}^2}\right) dt, \quad (24)$$

where  $I_0(\cdot)$  is the modified Bessel function of the first kind and order zero [22, Eq. (9.6.16)],  $\mathbf{m}_i = m_{\text{Re},i}^2 + m_{\text{Im},i}^2$ , and

$$\Omega_{p,i}^2 = \sigma_{p,i}^2 \left( \frac{1 - \lambda_{p,i}^2}{2} \right) \quad (25a)$$

$$\xi_i = 1 + \sum_{p=1}^2 \frac{\sigma_{p,i}^2 \lambda_{p,i}^2}{2\Omega_{p,i}^2}. \quad (25b)$$

#### IV. DOPPLER ANALYSIS

In this section, we provide a comprehensive statistical analysis on Doppler estimation. To do so, we derive the performance metrics for both SP and SP-plus-CCRT.

##### A. SP Analysis

First, let us define the following events:

$$\mathcal{A}_{k,i} = \{R_{1,i} > X_{k,i}\} \quad (26)$$

$$\mathcal{B}_{l,i} = \{R_{2,i} > Y_{l,i}\} \quad (27)$$

$$\mathcal{C}_{k,i} = \{X_{k,i} > R_{1,i}\} \quad (28)$$

$$\mathcal{D}_{l,i} = \{Y_{l,i} > R_{2,i}\}. \quad (29)$$

**Proposition I.** Let  $PD_i$  be the probability of detection at the  $i$ -th PRF. Specifically,  $PD_i$  is defined as the probability that  $R_{1,i}$  is greater than  $X_{k,i}$  and, simultaneously, that  $R_{2,i}$  is greater than  $Y_{l,i}$ , i.e.,

$$PD_i \triangleq \Pr \left[ \left( \bigcap_{k=1}^{M_i-1} \mathcal{A}_{k,i} \right) \cap \left( \bigcap_{l=1}^{N_i-1} \mathcal{B}_{l,i} \right) \right]. \quad (30)$$

Then, from (22)–(24), (30) can be expressed in closed-form as

$$PD_i = \sum_{k=0}^{M_i-1} \sum_{l=0}^{N_i-1} \binom{M_i-1}{k} \binom{N_i-1}{l} \times \frac{(-1)^{-k-l+M_i+N_i} \mathcal{V}_i(k,l)}{\mathcal{U}_i(k,l)} \exp\left(-\mathbf{m}_i + \frac{\mathbf{m}_i}{\mathcal{U}_i(k,l)}\right), \quad (31)$$

wherein  $\mathcal{U}_i(k,l)$  and  $\mathcal{V}_i(k,l)$  are auxiliary functions defined, respectively, as

$$\mathcal{U}_i(k,l) = \xi_i - \frac{\xi_i \lambda_{1,i}^2 \sigma_{1,i}^4}{2\Omega_{1,i}^2 (\Omega_{1,i}^2 (k - M_i + 1) - \sigma_{1,i}^2)} - \frac{\xi_i \lambda_{2,i}^2 \sigma_{2,i}^4}{2\Omega_{2,i}^2 (\Omega_{2,i}^2 (l - N_i + 1) - \sigma_{2,i}^2)} \quad (32a)$$

$$\mathcal{V}_i(k,l) = \frac{\sigma_{1,i}^2}{(\Omega_{1,i}^2 (-k + M_i - 1) + \sigma_{1,i}^2)} \times \frac{\sigma_{2,i}^2}{(\Omega_{2,i}^2 (-l + N_i - 1) + \sigma_{2,i}^2)}. \quad (32b)$$

*Proof.* See Appendix A. ■

**Corollary I.** Let  $PFA_i$  be the probability of false alarm at the  $i$ -th PRF. More precisely,  $PFA_i$  is defined as the probability that at least one of  $X_{k,i}$  is greater than  $R_{1,i}$  and, simultaneously, that at least one of  $Y_{l,i}$  is greater than  $R_{2,i}$ , i.e.,

$$PFA_i \triangleq \Pr \left[ \bigcup_{k=1}^{M_i-1} \bigcup_{l=1}^{N_i-1} (\mathcal{C}_{k,i} \cap \mathcal{D}_{l,i}) \right]. \quad (33)$$

Then, from (22)–(24), (33) can be written in closed-form as in (35), shown at the top of the next page, where  $\mathcal{P}_i(k,l)$  and  $\mathcal{Q}_i(k,l)$  are auxiliary functions defined, respectively, by

$$\mathcal{P}_i(k,l) = \xi_i - \frac{\lambda_{1,i}^2 \sigma_{1,i}^4}{2\Omega_{1,i}^2 (k \Omega_{1,i}^2 + \sigma_{1,i}^2)} - \frac{\lambda_{2,i}^2 \sigma_{2,i}^4}{2\Omega_{2,i}^2 (l \Omega_{2,i}^2 + \sigma_{2,i}^2)} \quad (34a)$$

$$\mathcal{Q}_i(k,l) = \frac{\sigma_{1,i}^2 \sigma_{2,i}^2}{(k \Omega_{1,i}^2 + \sigma_{1,i}^2) (l \Omega_{2,i}^2 + \sigma_{2,i}^2)}. \quad (34b)$$

*Proof.* See Appendix B. ■

It is worth mentioning that (31) and (35) are novel and original contributions of this work, derived in closed-form even though (24) is given in integral form.

##### B. SP-Plus-CCRT Analysis

Similar to [14], we assume that each individual pulse on each sweep results in an independent random value for the target returns.

Now, using (31) and taking into account the  $\mathcal{M}$ -of- $L$  detection criterion,<sup>5</sup> the probability of detection for the combined technique SP-plus-CCR can be calculated as follows [23]

$$PD_{\text{CCRT}} \triangleq \sum_{l=\mathcal{M}}^L \sum_{\mathcal{E} \in \mathcal{F}_l} \left\{ \left( \prod_{i \in \mathcal{E}} PD_i \right) \left( \prod_{j \in \mathcal{E}^c} (1 - PD_j) \right) \right\}, \quad (36)$$

where  $\mathcal{F}_l$  is the set of all subsets of  $l$  integers that can be selected from  $\{1, 2, \dots, L\}$ , and  $\mathcal{E}^c$  is the complement

<sup>5</sup>Instead of detecting a target on the basis of at least one detection in  $L$  tries, system designers often require that some number  $\mathcal{M}$  or more detections be required in  $L$  tries before a target detection is accepted [2].

$$\begin{aligned}
PFA_i = & \frac{(M_i - 1)(N_i - 1) Q_i(1, 1)}{\mathcal{P}_i(1, 1)} \exp\left(-\mathbf{m}_i + \frac{\mathbf{m}_i}{\mathcal{P}_i(1, 1)}\right) - \binom{M_i - 1}{2} \binom{N_i - 1}{2} \frac{Q_i(2, 2)}{\mathcal{P}_i(2, 2)} \exp\left(-\mathbf{m}_i + \frac{\mathbf{m}_i}{\mathcal{P}_i(2, 2)}\right) + \dots \\
& + (-1)^{M_i - N_i - 1} \frac{Q_i(M_i - 1, N_i - 1)}{\mathcal{P}_i(M_i - 1, N_i - 1)} \exp\left(-\mathbf{m}_i + \frac{\mathbf{m}_i}{\mathcal{P}_i(M_i - 1, N_i - 1)}\right)
\end{aligned} \quad (35)$$

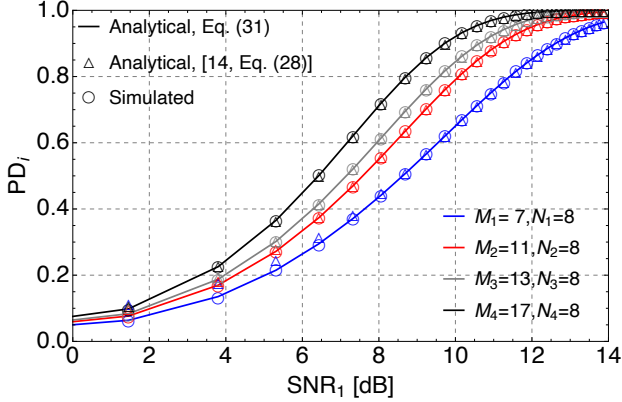


Fig. 2:  $PD_i$  vs  $SNR_1$  using  $N_i = 8$ ,  $\lambda_{1,i} = 0.5$ ,  $\lambda_{2,i} = 0.99$ , and different values of  $M_i$  ( $i \in \{1, 2, 3, 4\}$ ).

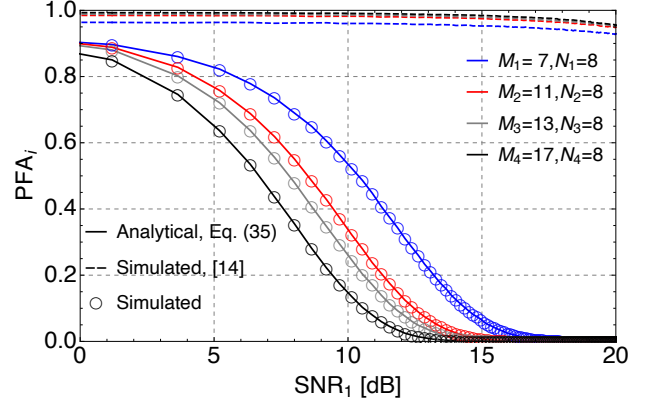


Fig. 3:  $PMD_i$  vs  $SNR_1$  using  $N_i = 8$ ,  $\lambda_{1,i} = 0.5$ ,  $\lambda_{2,i} = 0.99$ , and different values of  $M_i$  ( $i \in \{1, 2, 3, 4\}$ ).

of  $\mathcal{E}$ . For example, if  $l = 2$  and  $L = 3$ , then  $\mathcal{F}_2 = \{\{1, 2\}, \{1, 3\}, \{2, 3\}\}$ , and  $\mathcal{E}^c = \{1, 2, \dots, L\} \setminus \mathcal{E}$ .

On the other hand, the probability of false alarm for the combined technique SP-plus-CCRT can be calculated as [23]

$$PFA_{CCRT} \triangleq \sum_{l=\mathcal{M}}^L \sum_{\mathcal{E} \in \mathcal{F}_l} \left\{ \left( \prod_{i \in \mathcal{E}} PFA_i \right) \left( \prod_{j \in \mathcal{E}^c} (1 - PFA_j) \right) \right\}. \quad (37)$$

For the case where  $\mathcal{M} = L$ , (36) and (37) reduce, respectively, to

$$PD_{CCRT} = \prod_{i=1}^L PD_i \quad (38)$$

$$PFA_{CCRT} = \prod_{i=1}^L PFA_i. \quad (39)$$

## V. NUMERICAL RESULTS

In this section, we illustrate through Fig. 4 how the Doppler estimation process is carried out. Latter, we validate our derived expressions by means of Monte-Carlo simulations<sup>6</sup>. To do so, we make use of the following radar setup:  $PRF_1 = 700$  [Hz],  $PRF_2 = 1100$  [Hz],  $PRF_3 = 1300$  [Hz],  $PRF_4 = 1700$  [Hz],  $L = \mathcal{M} = 4$ ,  $f_R = 6$  [GHz],  $\tau = 25$  [ $\mu s$ ],  $\lambda = 0.05$  [m],  $M_1 = 11$ ,  $M_2 = 13$ ,  $M_3 = 17$ ,  $M_4 = 19$ , and  $N_i = 8 \forall i \in \{1, 2, 3, 4\}$ . In addition, we consider a linear frequency-modulated pulse with bandwidth  $B = 2$  [MHz].

Fig. 4 illustrates the output data after the 2D-DFT blocks. In this simulation example, we placed a target at an initial range of 10 [Km], traveling with a constant velocity of  $v_t = 900$

[m/s] in the opposite direction of the radar (i.e., the target is receding). Fig. 4(a) shows the normalized output data – Velocity vs Range – using PP. Observe that in all 4 scenarios, the target at 10 [Km] is unlikely to be detected due to the high loss in SNR. On the other hand, Fig. 4(b) shows the normalized output data – Velocity vs Range – using SP. Observe that the loss in SNR is partially mitigated by means of SP. Therefore, the target located at 10 [Km] can now be easily be detect without further processing. At last, Fig. 4(c) shows the combined pulse and subpulse information. Note in Fig. 4(c) that SP provides a better intuition about the target location, but due to its poor discretization, it is not sufficient to determine the exact velocity. Conversely, PP provides a better discretization but, unfortunately, its velocity estimation is more likely to be ambiguous. Thus, by combining SP and the CCRT, we provide the system a high capability to unfold the target's true velocity.

Fig. 2 shows  $PD_i$  versus  $SNR_1$  using different values of  $M_i$ . Note how radar performance improves as  $M_i$  increases, requiring a lower SNR for a given PD. This is because when increasing  $M_i$ , we are, in fact, increasing the compressed response of PP by means of coherent integration. In particular, for a fixed  $SNR_1 = 10$  [dB], we obtain the following probabilities of detection:  $PD_1 = 0.66$  for  $M_1 = 7$ ;  $PD_2 = 0.78$  for  $M_2 = 11$ ;  $PD_3 = 0.85$  for  $M_3 = 13$ ; and  $PD_4 = 0.93$  for  $M_4 = 17$ . Also, observe that for the high and medium SNR regime, our derived expression matches perfectly the PD of [14, Eq. (28)]. Nevertheless, there is a small difference in the PD for the low SNR regime. This occurs because if the compressed response of PP is less than the background noise, then the intersection probability in (30) will be less than the probability of  $\bigcap_{k=1}^{M_i-1} \mathcal{A}_{k,i}$ . For example, given  $SNR_1 = 4$  [dB] and  $M_1 = 7$ , we obtain  $PD_1 = 0.15$  with our proposed SP–

<sup>6</sup>The number of realizations in Monte-Carlo simulations was set to  $10^6$ .

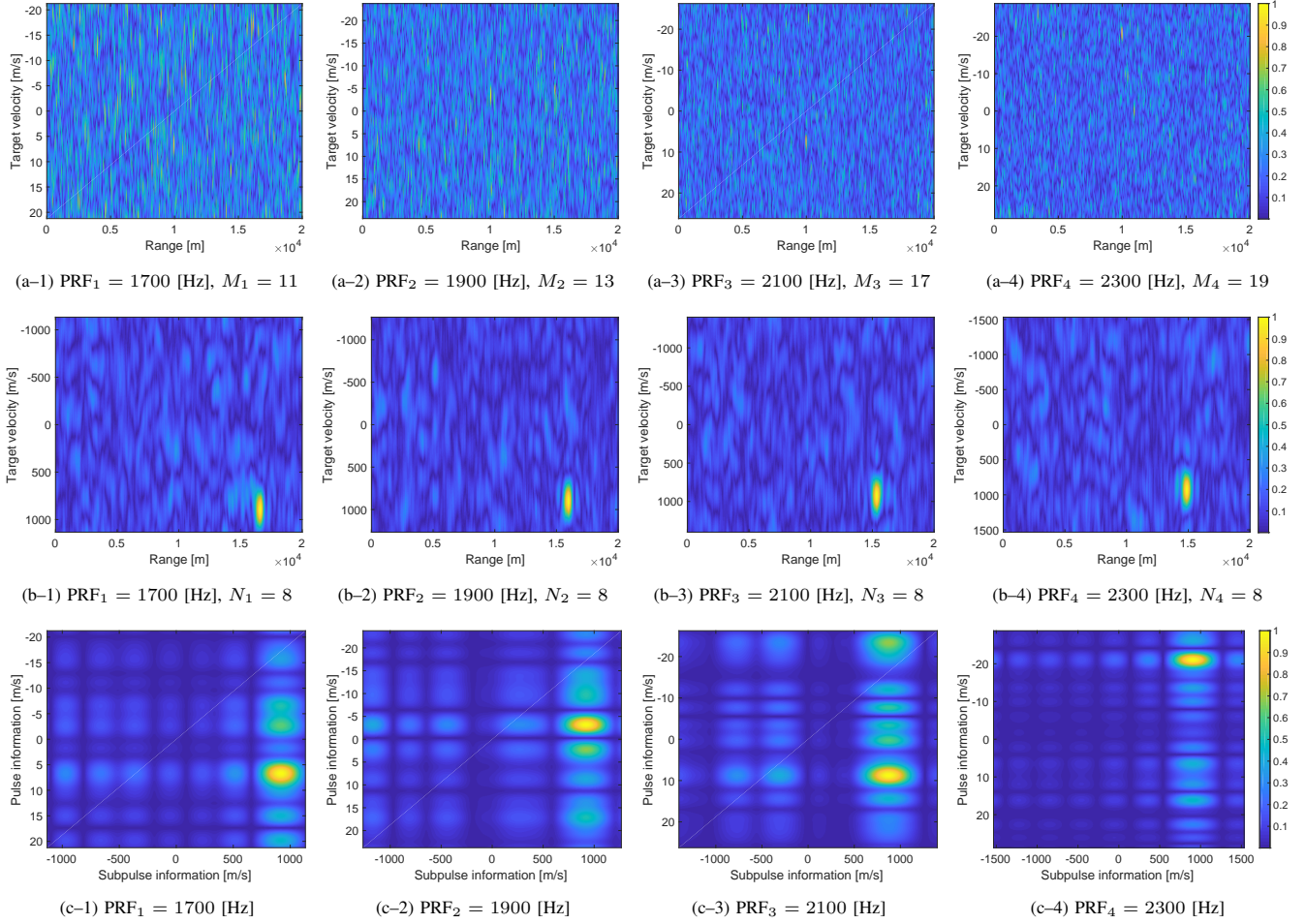
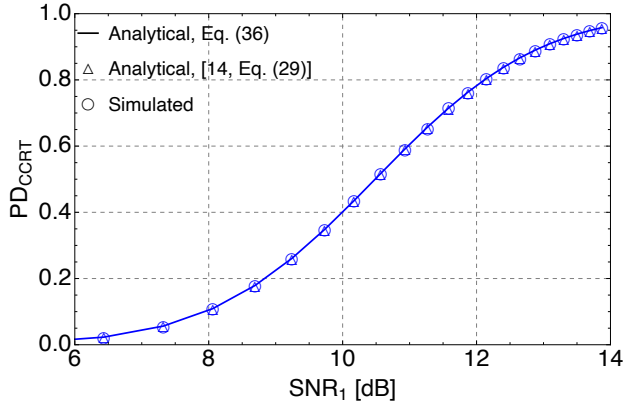
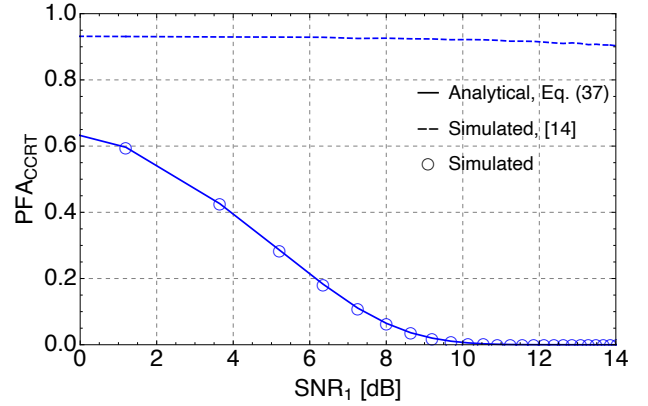


Fig. 4: Doppler estimation.

Fig. 5:  $PD_{CCRT}$  vs  $SNR_1$  using  $N_i = 8$ ,  $\lambda_{1,i} = 0.5$ ,  $\lambda_{2,i} = 0.99$ ,  $\mathcal{M} = 4$ , and different values of  $M_i$  ( $i \in \{1, 2, 3, 4\}$ ).Fig. 6:  $PMD_{CCRT}$  vs  $SNR_1$  using  $N_i = 8$ ,  $\lambda_{1,i} = 0.5$ ,  $\lambda_{2,i} = 0.99$ ,  $\mathcal{M} = 4$ , and different values of  $M_i$  ( $i \in \{1, 2, 3, 4\}$ ).

plus-CCRT technique, and  $PD_1 = 0.18$  with [14, Eq. (28)]. However, this small reduction in the PD is compensated by a greater reduction in the PFA, as shall be seen next.

Fig. 3 shows  $PFA_i$  versus  $SNR_1$  using different values for  $M_i$ . Observe how  $PFA_i$  decreases as  $M_i$  increases. This occurs because as we increase  $M_i$ , the received target echo becomes

stronger compared to the noise background. For example, for a fixed  $SNR_1 = 5$  [dB], we obtain the following probabilities of false alarm:  $PFA_1 = 0.83$  for  $M_1 = 7$ ;  $PFA_2 = 0.77$  for  $M_2 = 11$ ;  $PFA_3 = 0.73$  for  $M_3 = 13$ ; and  $PFA_4 = 0.60$  for  $M_4 = 17$ . More interesting, observe how  $PFA_i$  decays rapidly compared to [14]. This difference in  $PFA_i$  is because

intuitively SP acts as a backup detection process. That is, since the compressed response of SP is greater of the PP response (for high-velocity targets), then the probability in (33) is lower than the probability of  $\bigcup_{k=1}^{M_i-1} C_{k,i}$ . For example, using the classic PP technique [14], we obtain the following probabilities of false alarm:  $\text{PFA}_1 = 0.96$  for  $M_1 = 7$ ;  $\text{PFA}_2 = 0.97$  for  $M_2 = 11$ ;  $\text{PFA}_3 = 0.98$  for  $M_3 = 13$ ; and  $\text{PFA}_4 = 0.99$  for  $M_3 = 17$ .

Finally, Figs. 5 and 6 show  $\text{PD}_{\text{CCRT}}$  and  $\text{PFA}_{\text{CCRT}}$  versus  $\text{SNR}_1$ , respectively. Observe in Fig. 5, the perfect agreement between (36) and [14, Eq. (29)]. Hence, in this case, we have no advantage when using SP-plus-CCRT. On the other hand, observe in Fig. 6, the high difference in the PFA between of (37) and that in [14]. In this case, the use of SP-plus-CCRT improves radar performance by considerably reducing the false alarms. For instance, for given  $\text{SNR}_1 = 2$  [dB], we obtain probabilities of  $\text{PFA}_{\text{CCRT}} = 0.94$  using PP-plus-CCRT, and  $\text{PFA}_{\text{CCRT}} = 0.54$  using SP-plus-CCRT.

## VI. CONCLUSION

In this work, we provided a thorough statistical analysis on Doppler estimation when both SP and the CCRT were employed. To do so, we derived novel and closed-form expressions for the PD and PFA. Moreover, a comparison analysis between our proposed SP-plus-CCRT technique and the classic PP-plus-CCRT was carried out. Numerical results and Monte-Carlo simulations corroborated the validity of our expressions and showed that the PFA when using SP-plus-CCRT technique was greatly reduced compared to [14], thereby enhancing radar detection.

### APPENDIX A PROOF OF PROPOSITION I

Applying [24, Eq. (5.48)] and using the fact that  $X_{k,i}$  and  $Y_{l,i}$  are independent RVs, (30) can be rewritten as follows:

$$\begin{aligned} \text{PD}_i &= \int_0^\infty \int_0^\infty \left( \prod_{k=1}^{M_i-1} \Pr[X_{k,i} < r_{1,i} | R_{1,i} = r_{1,i}] \right) \\ &\quad \times \left( \prod_{l=1}^{N_i-1} \Pr[Y_{l,i} < r_{2,i} | R_{2,i} = r_{2,i}] \right) \\ &\quad \times f_{R_{1,i}, R_{2,i}}(r_{1,i}, r_{2,i}) \, dr_{1,i} \, dr_{2,i}. \end{aligned} \quad (40)$$

Now, with the aid of [24, Eq. (4.11)] and taking into account that  $X_{k,i}$  and  $Y_{l,i}$  are identically distributed RVs, yields

$$\begin{aligned} \text{PD}_i &= \int_0^\infty \int_0^\infty \left( \int_0^{r_{1,i}} f_{X_{1,i}}(x_{1,i}) \, dx_{1,i} \right)^{M_i-1} \\ &\quad \times \left( \int_0^{r_{2,i}} f_{Y_{1,i}}(y_{1,i}) \, dy_{1,i} \right)^{N_i-1} \\ &\quad \times f_{R_{1,i}, R_{2,i}}(r_{1,i}, r_{2,i}) \, dr_{1,i} \, dr_{2,i}. \end{aligned} \quad (41)$$

Replacing (22)–(24) in (41), we obtain

$$\begin{aligned} \text{PD}_i &= \int_0^\infty \int_0^\infty \underbrace{\left( \int_0^{r_{1,i}} \frac{x_{1,i} \exp\left(-\frac{x_{1,i}^2}{2\sigma_{1,i}^2}\right)}{\sigma_{1,i}} \, dx_{1,i} \right)^{M_i-1}}_{\triangleq \mathcal{I}_1} \\ &\quad \times \underbrace{\left( \int_0^{r_{2,i}} \frac{y_{1,i} \exp\left(-\frac{y_{1,i}^2}{2\sigma_{2,i}^2}\right)}{\sigma_{2,i}} \, dy_{1,i} \right)^{N_i-1}}_{\triangleq \mathcal{I}_2} \\ &\quad \times \int_0^\infty \exp(-\xi_i t) \exp(-\mathbf{m}_i) I_0(2\sqrt{\mathbf{m}_i t}) \\ &\quad \times \prod_{p=1}^2 \frac{r_{p,i}}{\Omega_{p,i}^2} \exp\left(-\frac{r_{p,i}^2}{2\Omega_{p,i}^2}\right) \\ &\quad \times I_0\left(\frac{r_{p,i} \sqrt{t\sigma_{p,i}^2 \lambda_{p,i}^2}}{\Omega_{p,i}^2}\right) \, dt \, dr_{1,i} \, dr_{2,i}. \end{aligned} \quad (42)$$

In order to solve (42), we must first evaluate  $\mathcal{I}_1$  and  $\mathcal{I}_2$ . In particular,  $\mathcal{I}_1$  can be calculated as follows:

$$\begin{aligned} \mathcal{I}_1 &\stackrel{(a)}{=} \left( 1 - \exp\left(-\frac{r_{1,i}^2}{2\sigma_{1,i}^2}\right) \right)^{M_i-1} \\ &\stackrel{(b)}{=} \sum_{k=0}^{M_i-1} \binom{M_i-1}{k} \left( -\exp\left(-\frac{r_{1,i}^2}{2\sigma_{1,i}^2}\right) \right)^{M_i-1-k}, \end{aligned} \quad (43)$$

where in step (a), we have developed the inner integral; and in step (b), we have used the binomial Theorem [24].

Using a similar approach to that used in (43),  $\mathcal{I}_2$  can be calculated as

$$\mathcal{I}_2 = \sum_{l=0}^{N_i-1} \binom{N_i-1}{l} \left( -\exp\left(-\frac{r_{2,i}^2}{2\sigma_{2,i}^2}\right) \right)^{N_i-1-l}. \quad (44)$$

Inserting (43) and (44) in (42), followed by changing the order of integration<sup>7</sup> and along with minor manipulations, we obtain (45), displayed at the top of the next page.

Now, it remains to find  $\mathcal{I}_3$  and  $\mathcal{I}_4$ . More precisely,  $\mathcal{I}_3$  can

<sup>7</sup>The change in the order of integration was performed without loss of generality since (22), (23) and (24) are non-negative real functions [25].



$$\begin{aligned}
\text{PD}_i &= \sum_{k=0}^{M_i-1} \sum_{l=0}^{N_i-1} 1^{k+l} \binom{M_i-1}{k} \binom{N_i-1}{l} \int_0^\infty \exp(-\xi_i t) \exp(-\mathbf{m}_i) I_0(2\sqrt{\mathbf{m}_i} t) \\
&\quad \times \underbrace{\int_0^\infty \left( -\exp\left(-\frac{r_{1,i}^2}{2\sigma_{1,i}^2}\right) \right)^{M_i-1-k} \frac{r_{1,i}}{\Omega_{1,i}^2} \exp\left(-\frac{r_{1,i}^2}{2\Omega_{1,i}^2}\right) I_0\left(\frac{r_{1,i}\sqrt{t\sigma_{1,i}^2\lambda_{1,i}^2}}{\Omega_{1,i}^2}\right) dr_{1,i}}_{\triangleq \mathcal{I}_3} \\
&\quad \times \underbrace{\int_0^\infty \left( -\exp\left(-\frac{r_{2,i}^2}{2\sigma_{2,i}^2}\right) \right)^{N_i-1-l} \frac{r_{2,i}}{\Omega_{2,i}^2} \exp\left(-\frac{r_{2,i}^2}{2\Omega_{2,i}^2}\right) I_0\left(\frac{r_{2,i}\sqrt{t\sigma_{2,i}^2\lambda_{2,i}^2}}{\Omega_{2,i}^2}\right) dr_{2,i} dt}_{\triangleq \mathcal{I}_4}. \tag{45}
\end{aligned}$$

be computed as

$$\begin{aligned}
\mathcal{I}_3 &\stackrel{(a)}{=} \int_0^\infty \left( -\exp\left(-\frac{r_{1,i}^2}{2\sigma_{1,i}^2}\right) \right)^{M_i-1-k} \frac{r_{1,i}}{\Omega_{1,i}^2} \\
&\quad \times \exp\left(-\frac{r_{1,i}^2}{2\Omega_{1,i}^2}\right) \sum_{q=0}^\infty \frac{\left(\frac{r_{1,i}\sqrt{t\lambda_{1,i}^2\sigma_{1,i}^2}}{2\Omega_{1,i}^2}\right)^{2q}}{q! \Gamma(q+1)} dr_{1,i} \\
&\stackrel{(b)}{=} \frac{(-1)^{-k+M_i+1}}{\Omega_{1,i}^2 \left(\frac{-k+M_i-1}{\sigma_{1,i}^2} + \frac{1}{\Omega_{1,i}^2}\right)} \\
&\quad \times \sum_{q=0}^\infty \frac{\left(\frac{t\lambda_{1,i}^2\sigma_{1,i}^4}{2\Omega_{1,i}^2(\Omega_{1,i}^2(-k+M_i-1)+\sigma_{1,i}^2)}\right)^q}{q!} \\
&\stackrel{(c)}{=} \frac{(-1)^{-k+M_i+1}}{\Omega_{1,i}^2 \left(\frac{-k+M_i-1}{\sigma_{1,i}^2} + \frac{1}{\Omega_{1,i}^2}\right)} \\
&\quad \times \exp\left(\frac{t\lambda_{1,i}^2\sigma_{1,i}^4}{2\Omega_{1,i}^2(\Omega_{1,i}^2(-k+M_i-1)+\sigma_{1,i}^2)}\right), \tag{46}
\end{aligned}$$

where in step (a), we have used the series representation of the modified Bessel function of the first kind and order zero [26, Eq. (03.02.02.0001.01)]; in step (b), we have solved the integral by first changing the order of integration; finally, in step (c), we have used [26, Eq. (01.03.06.0002.01)] and performed some algebraic manipulations.

In like manner as in (46),  $\mathcal{I}_4$  can be computed as

$$\begin{aligned}
\mathcal{I}_4 &= \frac{(-1)^{-l+N_i+1}}{\Omega_{2,i}^2 \left(\frac{-l+N_i-1}{\sigma_{2,i}^2} + \frac{1}{\Omega_{2,i}^2}\right)} \\
&\quad \times \exp\left(\frac{t\lambda_{2,i}^2\sigma_{2,i}^4}{2\Omega_{2,i}^2(\Omega_{2,i}^2(-l+N_i-1)+\sigma_{2,i}^2)}\right). \tag{47}
\end{aligned}$$

Now, replacing (46) and (47) in (45), we obtain

$$\begin{aligned}
\text{PD}_i &= \sum_{k=0}^{M_i-1} \sum_{l=0}^{N_i-1} \binom{M_i-1}{k} \binom{N_i-1}{l} \\
&\quad \times \exp(-\mathbf{m}_i) \left(\frac{\sigma_{1,i}^2(-1)^{-k+M_i+1}}{\Omega_{1,i}^2(-k+M_i-1)+\sigma_{1,i}^2}\right) \\
&\quad \times \left(\frac{\sigma_{2,i}^2(-1)^{-l+N_i+1}}{\Omega_{2,i}^2(-l+N_i-1)+\sigma_{2,i}^2}\right) \\
&\quad \times \int_0^\infty \exp(-\xi_i t) I_0(2\sqrt{\mathbf{m}_i} t) \\
&\quad \times \exp\left(\frac{t\lambda_{1,i}^2\sigma_{1,i}^4}{2\Omega_{1,i}^2(\Omega_{1,i}^2(-k+M_i-1)+\sigma_{1,i}^2)}\right) \\
&\quad \times \exp\left(\frac{t\lambda_{2,i}^2\sigma_{2,i}^4}{2\Omega_{2,i}^2(\Omega_{2,i}^2(-l+N_i-1)+\sigma_{2,i}^2)}\right) dt. \tag{48}
\end{aligned}$$

Finally, using the following identity [27, Eq. (1.11.2.4)]

$$\int_0^\infty \exp(tb) I_0(\sqrt{ta}) dt = -\frac{\exp\left(-\frac{a^2}{4b}\right)}{b}, \tag{49}$$

and after performing some minor simplifications, we can express (48) in closed-form as in (31), which completes the proof.

## APPENDIX B PROOF OF COROLLARY I

By making use of [24, Coroll. 6], we can express (33) as

$$\begin{aligned}
\text{PFA}_i &= \sum_{k=1}^{M_i-1} \sum_{l=1}^{N_i-1} \Pr\left[\mathcal{C}_{k,i} \cap \mathcal{D}_{l,i}\right] \\
&\quad - \sum_{k=1}^{M_i-1} \sum_{l=1}^{N_i-1} \sum_{p=2}^{M_i-1} \sum_{q=2}^{N_i-1} \Pr\left[\mathcal{C}_{k,i} \cap \mathcal{D}_{l,i} \cap \mathcal{C}_{p,i} \cap \mathcal{D}_{q,i}\right] + \dots \\
&\quad + (-1)^{M_i-N_i-1} \Pr\left[\mathcal{C}_{1,i} \cap \mathcal{D}_{1,i} \cap \dots \cap \mathcal{C}_{M_i-1,i} \cap \mathcal{D}_{N_i-1,i}\right]. \tag{50}
\end{aligned}$$

Now, we need to find the event probabilities. First, let us derive the last event probability of (50), that is,

$$\begin{aligned}
& \Pr \left[ \mathcal{C}_{1,i} \cap \mathcal{D}_{1,i} \cap \dots \cap \mathcal{C}_{M_i-1,i} \cap \mathcal{D}_{N_i-1,i} \right] \\
& \stackrel{a}{=} \int_0^\infty \int_0^\infty \left( \prod_{k=1}^{M_i-1} \Pr [X_{k,i} > r_{1,i} | R_{1,i} = r_{1,i}] \right) \\
& \quad \times \left( \prod_{l=1}^{N_i-1} \Pr [Y_{l,i} > r_{2,i} | R_{2,i} = r_{2,i}] \right) \\
& \quad \times f_{R_{1,i}, R_{2,i}}(r_{1,i}, r_{2,i}) \, dr_{1,i} \, dr_{2,i} \\
& \stackrel{b}{=} \int_0^\infty \int_0^\infty \left( \int_{r_{1,i}}^\infty f_{X_{1,i}}(x_{1,i}) \, dx_{1,i} \right)^{M_i-1} \\
& \quad \times \left( \int_{r_{2,i}}^\infty f_{Y_{1,i}}(y_{1,i}) \, dy_{1,i} \right)^{N_i-1} \\
& \quad \times f_{R_{1,i}, R_{2,i}}(r_{1,i}, r_{2,i}) \, dr_{1,i} \, dr_{2,i}, \tag{51}
\end{aligned}$$

where in step (a) we have used [24, Eq. (5.48)]; and in step (b) we have used [24, Eq. (4.11)] along with the fact that  $X_{k,i}$  and  $Y_{l,i}$  are identically distributed RVs.

Replacing (22)–(24) in (51), yields

$$\begin{aligned}
& \Pr \left[ \mathcal{C}_{1,i} \cap \mathcal{D}_{1,i} \cap \dots \cap \mathcal{C}_{M_i-1,i} \cap \mathcal{D}_{N_i-1,i} \right] \\
& = \int_0^\infty \int_0^\infty \underbrace{\left( \int_{r_{1,i}}^\infty \frac{x_{1,i} \exp\left(-\frac{x_{1,i}^2}{2\sigma_{1,i}^2}\right)}{\sigma_{1,i}} \, dx_{1,i} \right)^{M_i-1}}_{\triangleq \mathcal{I}_5} \\
& \quad \times \underbrace{\left( \int_{r_{2,i}}^\infty \frac{y_{1,i} \exp\left(-\frac{y_{1,i}^2}{2\sigma_{2,i}^2}\right)}{\sigma_{2,i}} \, dy_{1,i} \right)^{N_i-1}}_{\triangleq \mathcal{I}_6} \\
& \quad \times \int_0^\infty \exp(-\xi_i t) \exp(-\mathbf{m}_i) I_0(2\sqrt{\mathbf{m}_i} t) \\
& \quad \times \prod_{p=1}^2 \frac{r_{p,i}}{\Omega_{p,i}^2} \exp\left(-\frac{r_{p,i}^2}{2\Omega_{p,i}^2}\right) \\
& \quad \times I_0\left(\frac{r_{p,i} \sqrt{t\sigma_{p,i}^2 \lambda_{p,i}^2}}{\Omega_{p,i}^2}\right) \, dt \, dr_{1,i} \, dr_{2,i}. \tag{52}
\end{aligned}$$

After some mathematical manipulations,  $\mathcal{I}_5$  and  $\mathcal{I}_6$  can be calculated, respectively, as

$$\mathcal{I}_5 = \exp\left(-\frac{r_{1,i}^2(M_i-1)}{2\sigma_{1,i}^2}\right) \tag{53}$$

$$\mathcal{I}_6 = \exp\left(-\frac{r_{2,i}^2(N_i-1)}{2\sigma_{2,i}^2}\right). \tag{54}$$

Now, replacing (53) and (54) in (52), and after solving

remaining three integrals by applying the same procedure as in (48), we obtain

$$\begin{aligned}
& \Pr \left[ \mathcal{C}_{1,i} \cap \mathcal{D}_{1,i} \cap \dots \cap \mathcal{C}_{M_i-1,i} \cap \mathcal{D}_{N_i-1,i} \right] \\
& = \frac{\mathcal{Q}_i(M_i-1, N_i-1)}{\mathcal{P}_i(M_i-1, N_i-1)} \exp\left(-\mathbf{m}_i + \frac{\mathbf{m}_i}{\mathcal{P}_i(M_i-1, N_i-1)}\right), \tag{56}
\end{aligned}$$

where  $\mathcal{P}_i(k, l)$  and  $\mathcal{Q}_i(k, l)$  are auxiliary functions defined in (34), and the parameters  $k \in \{1, 2, \dots, M_i-1\}$  and  $l \in \{1, 2, \dots, N_i-1\}$  denote the number of events for  $\mathcal{C}_{k,i}$  and  $\mathcal{D}_{l,i}$ , respectively. Thus, the remaining event probabilities in (50) can be easily obtained by a proper choice of the parameters  $k$  and  $l$ . For example, for  $k=1$  and  $l=3$ , we obtain

$$\begin{aligned}
& \Pr \left[ \mathcal{C}_{1,i} \cap \mathcal{D}_{1,i} \cap \mathcal{D}_{2,i} \cap \mathcal{D}_{3,i} \right] \\
& = \frac{\mathcal{Q}_i(1, 3)}{\mathcal{P}_i(1, 3)} \exp\left(-\mathbf{m}_i + \frac{\mathbf{m}_i}{\mathcal{P}_i(1, 3)}\right), \tag{57}
\end{aligned}$$

whereas for  $k=3$  and  $l=2$ , we have

$$\begin{aligned}
& \Pr \left[ \mathcal{C}_{1,i} \cap \mathcal{D}_{1,i} \cap \mathcal{C}_{2,i} \cap \mathcal{D}_{2,i} \cap \mathcal{C}_{3,i} \right] \\
& = \frac{\mathcal{Q}_i(3, 2)}{\mathcal{P}_i(3, 2)} \exp\left(-\mathbf{m}_i + \frac{\mathbf{m}_i}{\mathcal{P}_i(3, 2)}\right). \tag{58}
\end{aligned}$$

Later, with the aid of (56) and after some algebraic manipulations, we can rewrite (50) as in (55), displayed at the top of the next page. Finally, and after minor simplifications, (55) reduces to (35), which completes the proof.

## REFERENCES

- [1] G. Morris and L. Harkness, *Airborne Pulsed Doppler Radar*, 2nd ed. Norwood, MA, USA: Artech House, 1996.
- [2] M. A. Richards, J. Scheer, W. A. Holm, and W. L. Melvin, *Principles of Modern Radar: Basic Principles*, 1st ed. West Perth, WA, Australia: SciTech, 2010.
- [3] G. V. Trunk, "Range resolution of targets using automatic detectors," *IEEE Trans. Aerosp. Electron. Syst.*, vol. AES-14, no. 5, pp. 750–755, Sept. 1978.
- [4] S. A. Hovanessian, "An algorithm for calculation of range in a multiple PRF radar," *IEEE Trans. Aerosp. Electron. Syst.*, vol. AES-12, no. 2, pp. 287–290, Mar. 1976.
- [5] X.-G. Xia and G. Wang, "Phase unwrapping and a robust chinese remainder theorem," *IEEE Signal Process. Lett.*, vol. 14, no. 4, pp. 247–250, Apr. 2007.
- [6] X. Li, H. Liang, and X. Xia, "A robust chinese remainder theorem with its applications in frequency estimation from undersampled waveforms," *IEEE Trans. Signal Process.*, vol. 57, no. 11, pp. 4314–4322, Nov. 2009.
- [7] W. Wang and X. Xia, "A closed-form robust chinese remainder theorem and its performance analysis," *IEEE Trans. Signal Process.*, vol. 58, no. 11, pp. 5655–5666, Nov. 2010.
- [8] G. V. Trunk and W. M. Kim, "Ambiguity resolution of multiple targets using pulse-Doppler waveforms," *IEEE Trans. Aerosp. Electron. Syst.*, vol. 30, no. 4, pp. 1130–1137, Oct. 1994.
- [9] F. D. A. García, A. S. Guerreiro, G. R. L. Tejerina, J. C. S. Santos Filho, G. Fraidenraich, M. D. Yacoub, M. A. M. Miranda, and H. Cioqueta, "Probability of detection for unambiguous doppler frequencies in pulsed radars using the chinese remainder theorem and subpulse processing," in *Proc. 53rd Asilomar Conference on Signals, Systems, and Computers*, Pacific Grove, CA, USA, Nov. 2019, pp. 138–142.
- [10] M. I. Skolnik, *Introduction to Radar Systems*, 3rd ed. New York, NY, USA: McGraw-Hill, 2001.
- [11] G. Beltrao, L. Pralon, M. Menezes, P. Vyplavin, B. Pompeo, and M. Pralon, "Subpulse processing for long range surveillance noise radars," in *Proc. International Conference on Radar Systems (Radar 2017)*, Belfast, UK, Oct. 2017, pp. 1–4.

$$\begin{aligned}
\text{PFA}_i = & \binom{M_i - 1}{1} \binom{N_i - 1}{1} \frac{\mathcal{Q}_i(1, 1)}{\mathcal{P}_i(1, 1)} \exp\left(-\mathbf{m}_i + \frac{\mathbf{m}_i}{\mathcal{P}_i(1, 1)}\right) - \binom{M_i - 1}{2} \binom{N_i - 1}{2} \frac{\mathcal{Q}_i(2, 2)}{\mathcal{P}_i(2, 2)} \exp\left(-\mathbf{m}_i + \frac{\mathbf{m}_i}{\mathcal{P}_i(2, 2)}\right) + \dots \\
& + (-1)^{M_i - N_i - 1} \binom{M_i - 1}{M_i - 1} \binom{N_i - 1}{N_i - 1} \frac{\mathcal{Q}_i(M_i - 1, N_i - 1)}{\mathcal{P}_i(M_i - 1, N_i - 1)} \exp\left(-\mathbf{m}_i + \frac{\mathbf{m}_i}{\mathcal{P}_i(M_i - 1, N_i - 1)}\right)
\end{aligned} \tag{55}$$

- [12] A. Barreto, L. Pralon, B. Pompeo, G. Beltrao, and M. Pralon, "FPGA design and implementation of a real-time subpulse processing architecture for noise radars," in *Proc. 2019 International Radar Conference (RADAR)*, Toulon, France, Sept. 2019, pp. 1–6.
- [13] D. S. Doviak and R. J. Zrnic, *Doppler Radar and Weather Observations*, 2nd ed. San Diego, CA, USA: Academic Press, 2001.
- [14] B. Silva and G. Fraidenraich, "Performance analysis of the classic and robust chinese remainder theorems in pulsed doppler radars," *IEEE Trans. Signal Process.*, vol. 66, no. 18, pp. 4898–4903, Sept. 2018.
- [15] M. A. Richards, *Fundamentals of Radar Signal Processing*, 2nd ed. Ney York, NY, USA: McGraw-Hill, 2014.
- [16] D. K. Barton, *Radar Equations for Modern Radar*, 1st ed. Massachusetts, MA, USA: Artech House, 2013.
- [17] G. Trunk and S. Brockett, "Range and velocity ambiguity resolution," in *Proc. Record IEEE Nat. Radar Conf.*, Lynnfield, MA, USA, Apr. 1993, pp. 146–149.
- [18] A. Ferrari, C. Berenguer, and G. Alengrin, "Doppler ambiguity resolution using multiple PRF," *IEEE Trans. Aerosp. Electron. Syst.*, vol. 33, no. 3, pp. 738–751, Jul. 1997.
- [19] A. Papoulis, *Probability, Random Variables, and Stochastic Processes*, 4th ed. Ney York, NY, USA: McGraw-Hill, 2002.
- [20] N. C. Beaulieu and K. T. Hemachandra, "Novel representations for the bivariate rician distribution," *IEEE Trans. Commun.*, vol. 59, no. 11, pp. 2951–2954, Nov. 2011.
- [21] A. Behnad, N. C. Beaulieu, and K. T. Hemachandra, "Correction to "Novel representations for the bivariate rician distribution"," *IEEE Trans. Commun.*, vol. 60, no. 6, pp. 1486–1486, Jun. 2012.
- [22] M. Abramowitz and I. A. Stegun, *Handbook of Mathematical Functions with Formulas, Graphs, and Mathematical Tables*. Washington, DC: US Dept. of Commerce: National Bureau of Standards, 1972.
- [23] Y. H. Wang, "On the number of successes in independent trials," *Statistica Sinica*, vol. 3, no. 2, pp. 295–312, 1993.
- [24] A. Leon-Garcia, *Probability and Random Processes for Electrical Engineering*, 3rd ed. New Jersey, NJ, USA: Pearson Prentice Hall, 1994.
- [25] H. Friedman, "A consistent Fubini-Tonelli theorem for nonmeasurable functions," *Illinois J. Math.*, vol. 24, no. 3, pp. 390–395, 1980.
- [26] Wolfram Research, Inc. (2018), *Wolfram Research*, Accessed: Sept. 19, 2018. [Online]. Available: <http://functions.wolfram.com>
- [27] A. P. Prudnikov, Y. A. Bryčkov, and O. I. Maričev, *Integral and Series: Vol. 2*, 2nd ed., Fizmatlit, Ed. Moscow, Russia: Fizmatlit, 1992.